Chinese Journal of Chemical Engineering 64 (2023) 106–116

Contents lists available at ScienceDirect

Chinese Journal of Chemical Engineering

journal homepage: www.elsevier.com/locate/CJChE

Full Length Article

Influence of support properties on selective oxidation of 2-methylnaphthalene on vanadia-molybdena based catalyst

Yi Yu [1], Fanfan Li [2], Xiaocong Li [3], Guoji Liu [1], Li Xu [1,*], Xingchuan Yang [1,*]

[1] School of Chemical Engineering, Zhengzhou University, Zhengzhou 450001, China
[2] School of Chemical and Printing-Dyeing Engineering, Henan University of Engineering, Zhengzhou 450007, China
[3] Kaifeng Wujing Industrial Co. Ltd, Kaifeng 475000, China

ARTICLE INFO

Article history:
Received 23 March 2023
Received in revised form 8 June 2023
Accepted 9 June 2023
Available online 4 July 2023

Keywords:
2-Methylnaphthalene
Catalysis
Partial oxidation
Support
Interactions

ABSTRACT

In this work, the catalytic performance of vanadia-molybdena loaded on TiO_2, MgO, ZSM-5, NaY and Mordenite was investigated in the selective oxidation of 2-methylnaphthalene (2-MN) to 2-naphthaldehyde (2-NA). Results show that strong interactions between supports (TiO_2, ZSM-5) and active components can promote the dispersion of active component. Monolayer VO_x and MoO_x are the main form on the catalyst surface, which is beneficial to the 2-NA selectivity. However, the corresponding weak interactions between Mordenite and active components may lead to the production of oxide crystals and the separation of active components, thus reducing the 2-NA selectivity. Due to the high Na content, new crystal $NaVMoO_6$ forms on the NaY surface, which is inactive in the reaction. For V-Mo/TiO_2, V and Mo can be inserted into the TiO_2 lattice, changing the electronic structures of active components and support and improving the activity of surface oxygen species. This investigation highlights an important consideration on supports properties when designing supported catalysts.

1. Introduction

Selective oxidation of hydrocarbons to their corresponding aldehydes, acids and anhydride is a primary reaction in fine chemical production. These oxygen functionalized intermediates are main raw materials to produce resins, rubber, fiber and polymer materials [1–3]. Unfortunately, industrial scale selective oxidation processes for the manufacture of most fine chemicals are still accomplished in toxic or caustic solvents by using the high-value metal salts such as potassium dichromate and potassium permanganate till now [4,5]. The resulting environmental problems have seriously affected the development of human society. Intense studies tried to develop new and environmentally friendly catalytic oxidation methods in recent years, which can effectively substitute conventional stoichiometric processes by using metal catalysts combined with green oxidants such as air, O_2 and H_2O_2 [6,7]. And lots of achievements have been made in developing new catalytic methods and catalysts, for example in the field of oxidation of ethane, propane and toluene. However, there still exists challenging in terms of achieving high conversion without over oxidation [8]. The selective oxidation of 2-methylnaphthalene (2-MN) to 2-naphthaldehyde (2-NA) is a typical example.

2-NA is an important intermediate to synthesize medicine, spices and pesticides [9,10]. It is manufactured industrially through the oxidation of 2-naphthalene nitrile or 2-naphthoyl chloride in liquid phase, which contains the characterizations of high production cost, equipment corrosion and harsh reaction conditions [11]. Our research group put forward and developed a greener gas–solid reaction method by oxidizing the cheap 2-MN, and vanadia-molybdena based catalysts exhibit excellent catalytic performance in this reaction [12,13].

For the supported vanadia-molybdena based catalysts, it is widely believed that active species morphology and supports properties are the two main factors that affect the catalytic performance [14,15]. As for the active component, the polymerized or isolated species usually exhibit different conversion and selectivity, and the reasons for these effects are still a controversial topic [16,17]. When comes to the selective oxidative dehydrogenation (ODH) of methanol and ethanol with two e^- reaction, the bridging V-O-support bond are considered as the active site, and the isolated and oligomeric active species show the highest active and selectivity. While for reactions involve the participation of O atom, the catalytic activity is proved to increase with the surface coverage of active components [18,19]. This conclusion is consistent

* Corresponding authors.
E-mail addresses: xuli@zzu.edu.cn (L. Xu), yangxingchuan@zzu.edu.cn (X. Yang).

https://doi.org/10.1016/j.cjche.2023.06.011
1004-9541/

with our previous research result that the most active and selective species are vanadia nearly monolayer covered on the support surface [12,13]. In this case, the active component is most affected by the support, avoiding various catalytic behaviors caused by exposure of different crystal planes on its surface. Excessive load of VO_x and MoO_x over one-monolayer capacity will result in the creation of V_2O_5 crystals, which is inactive in the oxidation reaction [20].

The status and activity of VO_x and MoO_x are also closely related to the nature of the support material. Kaichev *et al.* [21] reported the ODH of ethanol over vanadia supported on TiO_2, ZrO_2, Al_2O_3 and SiO_2 support, oxide monolayer are more likely to form on TiO_2 surface. While for ZrO_2, Al_2O_3 and SiO_2, the V_2O_5 crystallites exist regardless of the VO_x content because of the weak interactions. Wachs *et al.* [22] had put forward that the activity of surface VO_x can be associated with the Sanderson cation electronegativity of support. Schomäcker *et al.* [23] correlated the apparent activation energies of ODH of propane and methanol and suggested that the oxygen defect formation enthalpies or the reducibility of the active component can be used as a descriptor of its catalytic activity. However, studies on the influence of the support on the active component in the selective oxidation of aromatics have been rarely reported. In addition, the mechanism of the effect of different support surface properties on the dual active components (VO_x/MoO_x) remains unclear.

Herein, in this work, we dispersed VO_x and MoO_x on five different materials with different surface properties and pore structure. These catalysts were applied in the gas–solid oxidation of 2-MN to 2-NA in order to evaluate how support materials and properties affect catalysts behavior in this reaction.

2. Experimental

2.1. Catalysts preparation

Anatase TiO_2 (99.8%) and MgO (99.0%) were supplied by Macklin reagent company. ZSM-5 (Si/Al = 25), NaY (Si/Al = 5) and Mordenite (Si/Al = 25) were bought from Nankai Catalyst Company. In a typical synthesis process, a certain amount of NH_4VO_3 (99%, Macklin) and $(NH_4)_6Mo_7O_{24}{\cdot}4H_2O$ (99%, Macklin) were dissolved in aqueous oxalate solution. Then, certain amounts of promoters K_2SO_4 and $K_2S_2O_7$ were dissolved. After different supports impregnation, the catalysts were dried at 110 °C overnight. Subsequently, they were calcined at 500 °C for 2 h in air. The load of V is 5.8%(mass), which has been proved the optimal value in this reaction. The molar ratio of V to Mo is 1:1.

2.2. Catalyst characterization

The X-ray powder diffraction (XRD) was measured on a Bruker D8 Advance diffractometer with Cu K_α radiation. Texture properties of different catalysts were measured by Quantachrome iQ2. 0.2 g samples were pretreated at 300 °C under vacuum before testing. Fourier transform infrared (FTIR) spectra were determined by Perkin-Elmer Spectrum GX in the range of 4000–400 cm^{-1}. Raman spectroscopy measurements were recorded by LabRAM HR Evo spectrometer with a 514 nm maser. TEM and HRTEM were performed by TalosF200 FEI with an accelerating voltage of 200 kV.

Chemisorption of NH_3 or O_2 was measured by using a TP-5080D instrument (Xianquan, Tianjin). For the NH_3-TPD measurement, 0.1 g catalysts were pretreated at 300 °C in a He atmosphere. Then, the catalyst was subsequently cooled to 80 °C and saturated with the NH_3/He blend (20% (vol)). After the desorption of physically adsorbed NH_3 at 110 °C, TCD signals were collected from 80 to 550 °C at 10 °C·min^{-1}. For O_2-TPD, 0.1 g catalysts were pretreated at 300 °C, and then placed in an atmosphere of oxygen. When the desorption of physisorbed oxygen is complete, the experiment was performed from 80 to 1000 °C. H_2-TPR was performed by the same equipment, 0.1 g catalysts were heated in N_2 atmosphere at 300 °C. After the catalysts were cooled to room temperature, the TPR was proceed in H_2/N_2 (5% (vol)) atmosphere from 30 to 900 °C at 10 °C·min^{-1}. XPS was measured on Thermo Fisher Scientific ESCALAB 250Xi instrument with Al K_α irradiation. The binding energies were calibrated by using carbon 1 s peak at 284.8 eV.

2.3. Activity testing

Partial oxidation of 2-MN was carried out in a continuous-flow fixed-bed reactor with a stainless steel reaction tube (10 mm I.D.). Before testing, all catalysts were pressed into wafers, crushed and sieved to a pellet size between 0.18 and 0.23 nm. Typically, 0.5 g catalysts mixed with 2.5 g silica sand with the same particle size were loaded in the isothermal zone of reaction tube. A type K thermocouple was placed at the vertical center of the catalyst bed to monitor the actual temperature. The catalysts were pretreated under air atmosphere at 400 °C for 2 h before exposing them to the reactants. After the pretreatment, 2-MN was evaporated into the air stream by bubbling at 120 °C. All gas transfer lines were wrapped in heating strips and kept at 150 °C to prevent the liquidation and condensation of reactant gas (molar ratio of 2-MN to O_2 was 1:160). The flow of reactant mixture was adjusted by mass flow controller and the gas hourly space velocity (GHSV) was kept at 10000 h^{-1}. Chemical species in the feed and reactor effluent stream were absorbed by 1,4-dioxane and quantitatively measured by gas chromatograph (Agilent 7890B) equipped HP-5 column. Black experiment results showed that the steel reaction tube and silica sand had no catalytic ability for 2-MN. Each set of experiment at a certain temperature was repeated three times for the average. The 2-MN conversion (%), 2-NA selectivity (%) and 2-NA yield (%) were calculated based on the inlet and out let concentrations:

$$\text{2-MN conversion} = (\text{2-MN}_{in} - \text{2-MN}_{out})/\text{2-MN}_{in} \times 100\%$$

$$\text{2-NA selectivity} = \text{2-NA}_{out}/\text{2-MN}_{converted} \times 100\%$$

$$\text{2-NA yield} = \text{2-MN conversion} \times \text{2-NA selectivity}/100\%$$

where 2-MN_{in}, 2-MN_{out}, 2-NA_{out} and $\text{2-MN}_{converted}$ represent the inlet 2-MN moles, the outlet 2-MN moles, the outlet 2-NA moles and the converted 2-MN moles.

2.4. Theoretical calculations

Mulliken charges and projected density of state (PDOS) of V-Mo/TiO_2 catalyst was calculated by using Materialsstudio 2017. Catalysts structural optimizations were performed using the GGA-PBE exchange correlation functional form and DNP basis set. Monolayer VO_x and MoO_x were placed on a two layer (4 × 2) TiO_2 (0 0 1) surface to simulate catalyst system. The vacuum space of all models was set 2 nm. *K*-points mesh used to optimize the super cell is 3 × 2 × 1.

3. Results and Discussion

3.1. Catalytic activity

In this reaction, apart from the target 2-NA, the main by-products were ring-opening phthalic anhydride, 4-methylphthalic anhydride and 2-methyl-1,4-naphthoquinone. Fig. 1 shows the catalytic performances of V-Mo/ZSM-5, V-Mo/

NaY, V-Mo/Mordenite, V-Mo/MgO and V-Mo/TiO_2. Within the range of reaction temperature 370–410 °C, the 2-MN conversion over V-Mo/MgO is always lower than 20%, and no target 2-NA is produced. It can be considered that MgO support used for selective oxidation of alkanes is not active in this reaction. At temperatures range from 340 to 410 °C, V-Mo/TiO_2 shows the highest activity, followed by V-Mo/Mordenite > V-Mo/ZSM-5 > V-Mo/NaY. From Fig. 1(b), 2-NA selectivity over V-Mo/TiO_2 is lower than that over V-Mo/zeolite catalysts at 340–360 °C, indicating that V-Mo/TiO_2 can achieve better performance only at a certain temperature. At temperatures 360–390 °C, the 2-NA selectivity over V-Mo/TiO_2 remains at a high level, while it decreases markedly for V-Mo/zeolite catalysts. V-Mo/TiO_2 presents the highest yield 35.31% of 2-NA at temperature 390 °C.

Since the catalysts are being developed for use in fine chemical production, the catalytic stability of the optimal V-Mo/TiO_2 catalyst was measured and the results are shown in Fig. 2. At the optimum reaction temperature of 390 °C, the 2-NA yield remains about 35% for a long time. After 40 h of reaction, the reaction temperature is reduced to 360 °C and the 2-NA yield maintains at around 18%. When the reaction is carried out for 60 h, the catalyst performance does not change significantly after the reaction temperature is increased to 390 °C. These indicate that V-Mo/TiO_2 catalyst has strong catalytic stability.

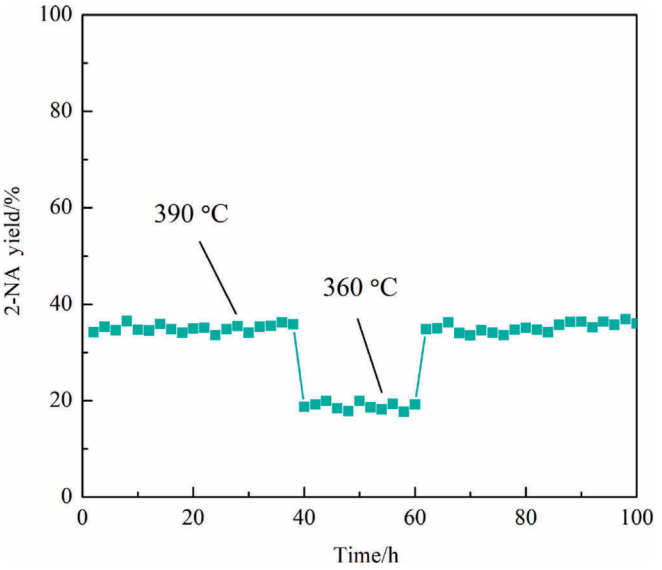

Fig. 2. Stability test of V-Mo/TiO_2 in the oxidation of 2-MN.

3.2. Structural properties

In order to explore the existence forms of active components VO_x and MoO_x, the catalysts were characterized by XRD. From Fig. 3, peaks representing support materials can be observed for all catalysts. There are no obvious V_2O_5 and MoO_3 diffraction peaks for V-Mo/TiO_2, indicating the surface VO_x and MoO_x are well dispersed or in the amorphous structure [24,25]. A few characteristic peaks of VO_2 (JCPDS PDF#76-0673) can be detected for V-Mo/ZSM-5 and peaks of V_2MoO_8 (JCPDS PDF#47-1081) can be identified for V-Mo/MgO, suggesting that the dispersion of active components decreases on these two supports. While for V-Mo/NaY and V-Mo/Mordenite, the peaks of V_2O_5 (JCPDS PDF#45-1074) and MoO_3 (JCPDS PDF#47-1081) are even observed, showing that the dispersion of VO_x and MoO_x on these two supports is poor. For V-Mo/NaY, diffraction peaks of a new ternary phase $NaVMoO_6$ instead of support are observed, this indicates that high content of Na can react with VO_x and MoO_x during the catalysts preparation process. In addition, the peaks of $AlVMoO_7$ are also detected. $MgMoO_4$, the

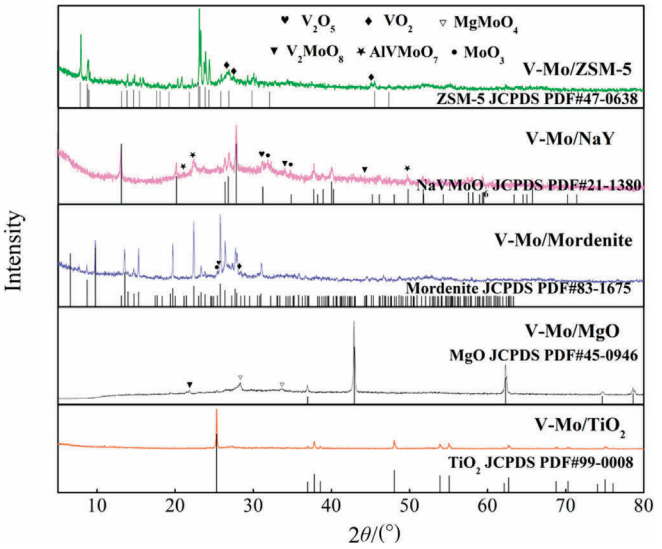

Fig. 3. XRD patterns of catalysts with different supports.

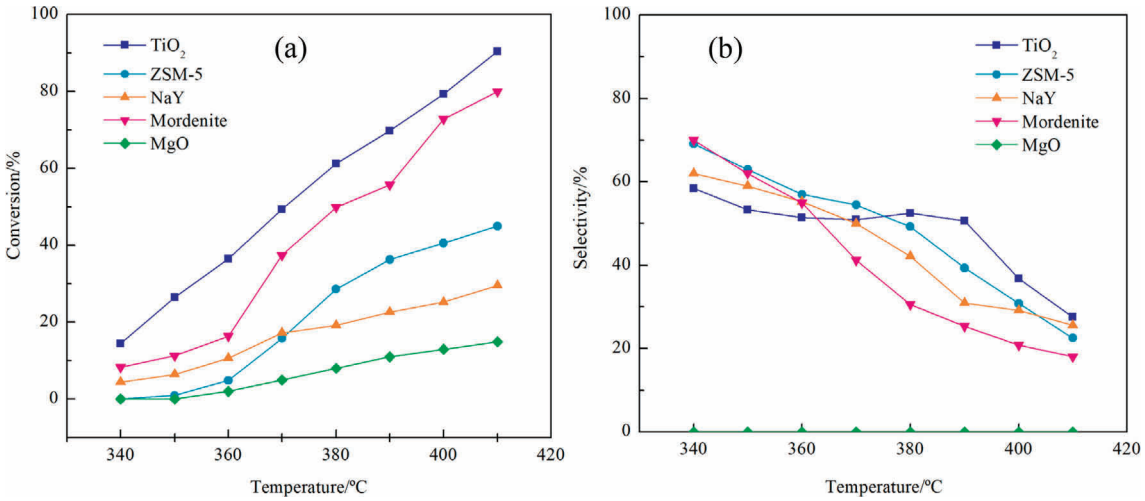

Fig. 1. 2-MN conversion (a) and 2-NA selectivity (b) on different catalysts.

product of the reaction between MgO and Mo, is also found for V-Mo/MgO [26]. Studies have shown that the active component dispersion on the support surface is related to the interaction strength between them [27]. Hence, VO_x and MoO_x monolayer tend to form on the TiO_2 surface due to the strong interaction, so as to ZSM-5. While the V_2O_5 and MoO_3 crystals are easily formed on the NaY and Mordenite surface even when the V and Mo loading is lower than that of monolayer, which is due to the weak interaction [28]. In addition, the appearance of crystallization on zeolites may due to the presence of more microporous structures in the material, which hinders the diffusion of active ions during the impregnation process. The strong alkali properties of MgO promote the dispersion of acidic active components on its surface to some extent. As a result, only a small number of crystals exist from Fig. 3.

Studies on vanadia based catalysts have shown that crystalline VO_x species, especially V_2O_5 crystals, are not favorable for selective oxidation, because V_2O_5 formed on the support will expose different crystal faces and thus has different selectivity for various products [29,30]. MoO_3 also has this feature. Moreover, V_2O_5 and MoO_3 crystals show more inactive when compared with monolayer dispersed active species in the reports of toluene and *p*-xylene selective oxidation [31,32]. Catalytic testing results in this study also confirm this conclusion, that V-Mo/TiO_2 has the optimal catalytic performance. And 2-NA selectivity over V-Mo/ZSM-5 with less oxide crystals was higher than that over V-Mo/NaY and V-Mo/Mordenite. However, the 2-MN conversion of V-Mo/ZSM-5 is relatively low, indicating that the dispersion of active components is only one factor affecting the activity.

In order to more intuitively distinguish the presence form of active components on the surface of TiO_2 and zeolite supports. The morphology of V-Mo/TiO_2 and V-Mo/NaY were characterized through TEM and HRTEM. From Fig. 4(a_1)–(a_5), no obvious aggregation and corresponding oxide crystals are found. In addition, only the anatase TiO_2 phase can be detected as they are identified by the spacing distance of 0.35 from (1 0 1) planes in Fig. 4(a_6). These demonstrate that VO_x and MoO_x exist in a highly dispersed form on TiO_2 surface. While for V-Mo/NaY, there are a lot of fine particles around the support crystals from Fig. 4(b_1). These particles are confirmed $NaVMoO_6$ crystals due to the pacing distance of 0.32 nm from (−1 1 1) planes. In addition, EDS-mapping in Fig. 4(b_4)–(b_6) shows that the dispersion of crystal particles on NaY surface is uniform.

Table 1 shows the texture values of V-Mo/support. Catalysts exhibit the higher BET surface area when zeolites are used as support, V-Mo/NaY shows the largest surface area 456 $m^2 \cdot g^{-1}$, while V-Mo/TiO_2 has the smallest value (4.33 $m^2 \cdot g^{-1}$) among catalysts. Active components dispersion is usually related to the surface area of catalyst, and larger value will be more conductive to the metal oxides dispersion. However, in this study, the dispersion of VO_x and MoO_x on the zeolites with large specific surface area is not as good as that of TiO_2, indicating that the polymerization degree of VO_x and MoO_x is strongly affected by VO_x/MoO_x-support interactions for these catalysts [26]. The pore properties of catalysts also affect the diffusion of reactants and products molecules. Catalysts with zeolites as support show typical microporous and mesoporous characteristics. For V-Mo/ZSM-5 and V-Mo/NaY, the micropores surface area and volume account for more than 50% of the total value, respectively. The molecular diameters of 2-MN and 2-NA are both larger than 0.7 nm. While the average pore sizes of V-Mo/ZSM-5 and V-Mo/NaY are 1.69 and 2.54 nm, which would inhibit reactants and product molecules diffusion in the pore during the reaction. Because the α position on the naphthalene ring of 2-MN is also active, the narrow pore makes the naphthalene ring more likely to collide with the active site, which leads to the ring opening reaction to produce anhydride rather than 2-NA. In addition, with the increase of reaction temperature, the thermal

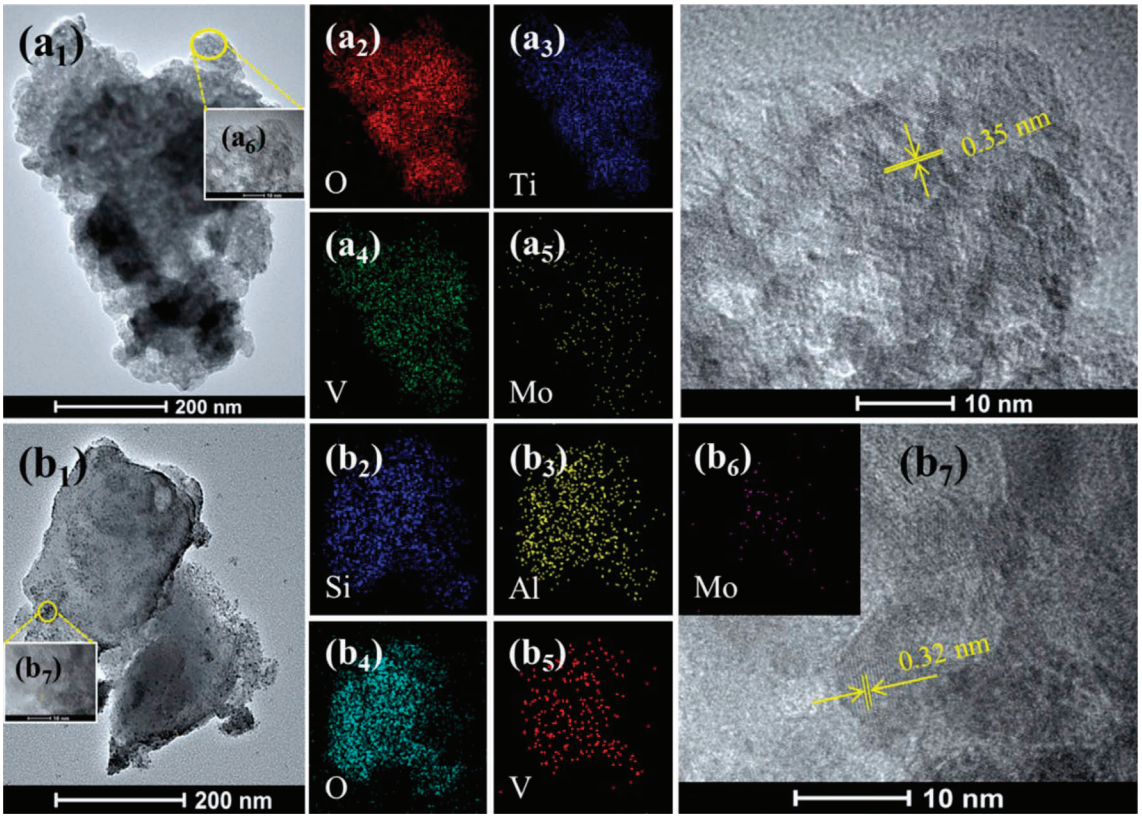

Fig. 4. TEM, HRTEM and EDS-mapping images of (a) V-Mo/TiO_2 and (b) V-Mo/NaY.

Table 1
The texture values of catalysts with different supports

Catalysts	S_{total}①/$m^2 \cdot g^{-1}$	S_{micro}②/$m^2 \cdot g^{-1}$	S_{meso}③/$m^2 \cdot g^{-1}$	V_{micro}④/$cm^3 \cdot g^{-1}$	V_{meso}⑤/$cm^3 \cdot g^{-1}$	D⑥/nm
V-Mo/ZSM-5	151	141	10	0.05	0.01	1.69
V-Mo/NaY	456	364	92	0.15	0.14	2.54
V-Mo/Mordenite	153	87	46	0.04	0.07	3.31
V-Mo/MgO	24	–	24	–	0.11	19.15
V-Mo/TiO_2	4	–	4	–	0.11	28.36

① Surface area calculated by BET method.
② Microporous surface area calculated by *t*-plot method.
③ Microporous surface area calculated by $S_{total} - S_{micro}$.
④ Microporous volume calculated by *t*-plot method.
⑤ Mesoporous volume calculated by $V_{total} - V_{micro}$.
⑥ Average pore size.

motion intensifies, making the aromatic ring easier to contact with the active site. V-Mo/TiO_2 and V-Mo/MgO contain only mesoporous surface area and pore volume without micropores based on *t*-plot method, which is benefit for the improvement of 2-NA selectivity. However, V-Mo/MgO has almost no catalytic activity and 2-NA selectivity, suggesting that other surface properties of this catalyst are not conducive to the gas phase oxidation of 2-MN.

3.3. Vibrational character

Fig. 5 displays FTIR spectra of V-Mo/Support catalysts. Absorption peaks at 3500 and 1630 cm^{-1} represent the O—H and H—O—H of physical adsorbed water. The wide peak between 500 and 900 cm^{-1} of V-Mo/TiO_2 represents the bending vibration of Ti—O—Ti in anatase TiO_2 [33]. Peaks at about 1070 and 458 cm^{-1} of V-Mo/Mordenite, V-Mo/ZSM-5 and V-Mo/NaY belong to the stretching and bending vibration of Si—O—Si in silica [34]. All catalysts contain characteristic peak of 1410 cm^{-1} that represents the asymmetric stretching vibration of covalent sulfate species formed by sulfur oxide and support, indicating that the added promoter K_2SO_4 in the preparation process can interact with different supports [33]. For V-Mo/TiO_2, peaks at about 1200 cm^{-1} representing the interaction between VO_x, support and sulfuric acid species can be observed. But in zeolites support catalysts, this peak has some degrees of deviation, indicating differences in interaction between active components and support. Small peak at 1030 cm^{-1} of V-Mo/TiO_2 belongs to the terminal V=O in crustal V_2O_5, indicating that there are a small amount of V_2O_5 microcrystals on the surface of V-Mo/TiO_2, which cannot be detected by XRD [14]. The infrared spectra of the three zeolites support catalysts do not contain this absorption peak, which may due to the covering by peak of support. For V-Mo/TiO_2, peak at 960 cm^{-1} indicates that VO_x mainly exists in the form of monolayer [35]. However, it disappears in the infrared spectra of the zeolites support catalysts. Peak at 786 cm^{-1} representing V—O—Mo bond cannot be found for V-Mo/TiO_2, which may due to the strong characteristic peak of support [36].

The weak absorption peak at 910 cm^{-1} represents terminal Mo=O in surface MoO_x [37]. The larger intensity of this peak for V-Mo/zeolites, especially for V-Mo/NaY, demonstrates the low dispersion of MoO_x. The absorption peak at 725 cm^{-1} in V-Mo/NaY represents the characteristic vibration of V—O—Al in $AlVMoO_7$ solid solution [27]. But it disappears in V-Mo/ZSM-5 and V-Mo/Mordenite, which may due to the low Al content in these zeolites.

Raman spectra of V-Mo/TiO_2, V-Mo/ZSM-5 and V-Mo/NaY were characterized to acquire more detailed structural information about surface active components. From Fig. 6, characteristic peaks corresponding to the surface active components of the catalysts are mainly in the range 700–1000 cm^{-1}. Peak at 771 cm^{-1} represents the vibration of V—O—Mo bond [38]. When compared with V-Mo/NaY, the peak intensity of V-Mo/TiO_2 and V-Mo/ZSM-5 is larger, indicating that the interaction between the active components VO_x and MO_x over TiO_2 and ZSM-5 is stronger than that over NaY. The peak near 990 cm^{-1} represents the terminal Mo=O or V=O bond. And peaks near 842 and 950 cm^{-1} reflect the V—O—V and Mo—O—Mo bonds in two-dimensional form on the catalyst surface [39,40]. The intensity of these two characteristic peaks for NaY is weak, which may result from the surface crystals.

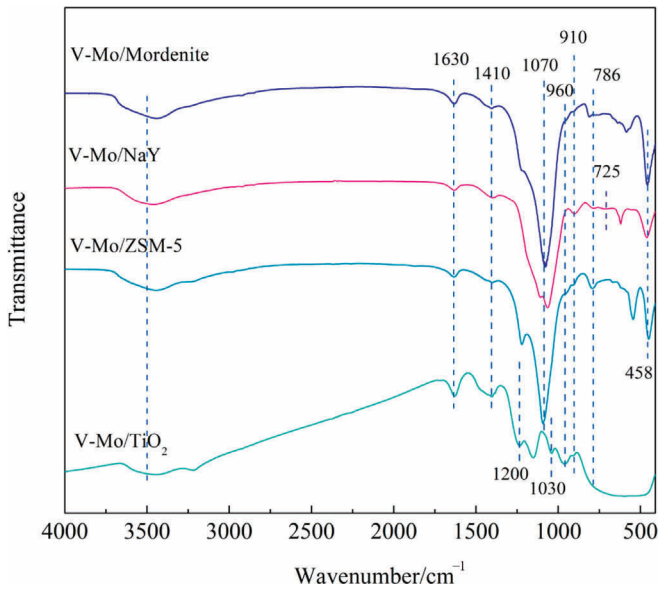

Fig. 5. FTIR spectra of catalysts with different supports.

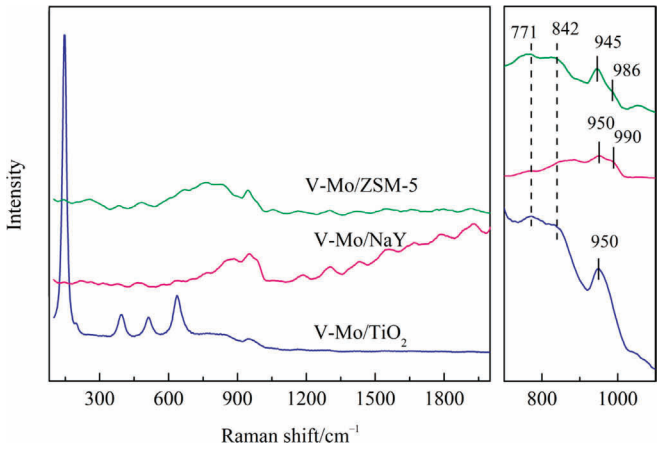

Fig. 6. Laser Raman spectra of different catalysts.

3.4. Acidic properties

Acidic properties of V-Mo/TiO_2 were studied by NH_3-TPD. From Fig. 7(a), V-Mo/Mordenite and V-Mo/ZSM-5 catalysts contain two ammonia desorption peaks at 220 and 350 °C, corresponding to weak and dium-strong acid sites [41]. V-Mo/Mordenite contains larger number of the two acid sites compared with V-Mo/ZSM-5. V-Mo/NaY contains a large amount of weak and few dium-strong acid sites, this may due to weak acidity of Al_2O_3 in the zeolite framework [42]. When compared to V-Mo/Mordenite, V-Mo/TiO_2 shows weaker acid strength and smaller number of acid sites. V-Mo/MgO almost contains no NH_3 desorption peaks, which is related to the basic properties of MgO, resulting in the poor catalytic performance in 2-MN oxidation. For zeolites supported catalysts, 2-MN conversion is positively related to the acid sites numbers. However, catalyst V-Mo/TiO_2 with relatively small amount of acid sites displays much higher activity. To explain this phenomenon, three pure zeolites were characterized by NH_3-TPD.

From Fig. 7(b), Mordenite and ZSM-5 contain two peaks at about 200 and 480 °C, demonstrating weak and strong acid sites. While NaY contains peaks at 280 and 330 °C, ascribable to weak and dium-strong acid sites. To contrast TPD patterns in Fig. 7(a) and (b), it can be concluded that active components VO_x and MoO_x occupy part of the acid sites of supports. And the surface acid sites of V-Mo/TiO_2 are derived from the dispersed active component. The acid sites of V-Mo/Mordenite, V-Mo/ZSM-5 and V-Mo/NaY are derived not only from active component but also from the supports [43]. According to the active testing results, large number of strong acid sites may cause the low 2-NA selectivity over V-Mo/Mordenite. And the low activity of V-Mo/NaY may result from the insufficient dium-strong acid sites [14]. These phenomena are consistent with our previous result that weak and dium-strong acid sites need to maintain a certain ratio [13]. In addition, the strong acidic skeleton aluminum in zeolite has a strong adsorption effect on aromatic aldehydes, leading to the difficulty of desorption of them from the catalyst surface [44]. Therefore, the selectivity of 2-NA decreases sharply at high temperatures on the corresponding catalysts.

3.5. Reducibility

In the process of temperature-programmed reduction, excessive temperature will cause transformation in the catalyst crystal structure. For example, peaks near 800 °C may result from the speciation of V_2O_5 crystals from polymerized vanadia at high temperature [45]. Therefore, we only analyze the reduction peak before 800 °C in H_2-TPR spectra (Fig. 8). Except for V-Mo/Mordenite, the H_2-TPR curves of the other three catalysts only contain a reduction peak in a large temperature range, and there is no relatively isolated reduction peak of vanadia and molybdena species, indicating that the interaction between VO_x and MoO_x of these three catalysts is stronger than that of V-Mo/Mordenite. The one main peak can be attributed the overlap of reduction peaks of VO_x and MoO_x, including V^{5+} to V^{4+} and V^{3+}, and Mo^{6+} to Mo^{5+} [42,43]. Reduction peaks for V-Mo/ZSM-5 and V-Mo/TiO_2 at around 584 and 612 °C can be assigned to the monolayer VO_x and MoO_x [45]. V-Mo/TiO_2 shows higher reduction temperature than V-Mo/ZSM-5, which may result from the strong interactions between VO_x/MoO_x and TiO_2 [42]. Previous studies suggested the interaction between MoO_x and support could promote the electron transfer process between support and VO_x, such interaction would lead to the reduced reducibility of

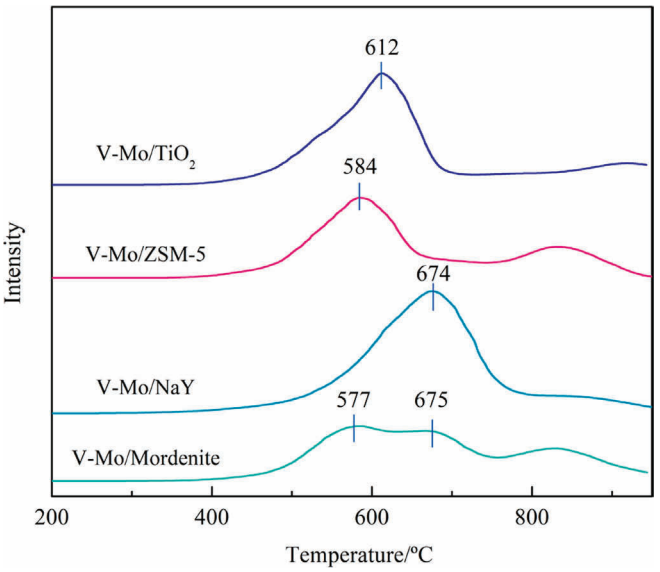

Fig. 8. H_2-TPR spectra of different catalysts.

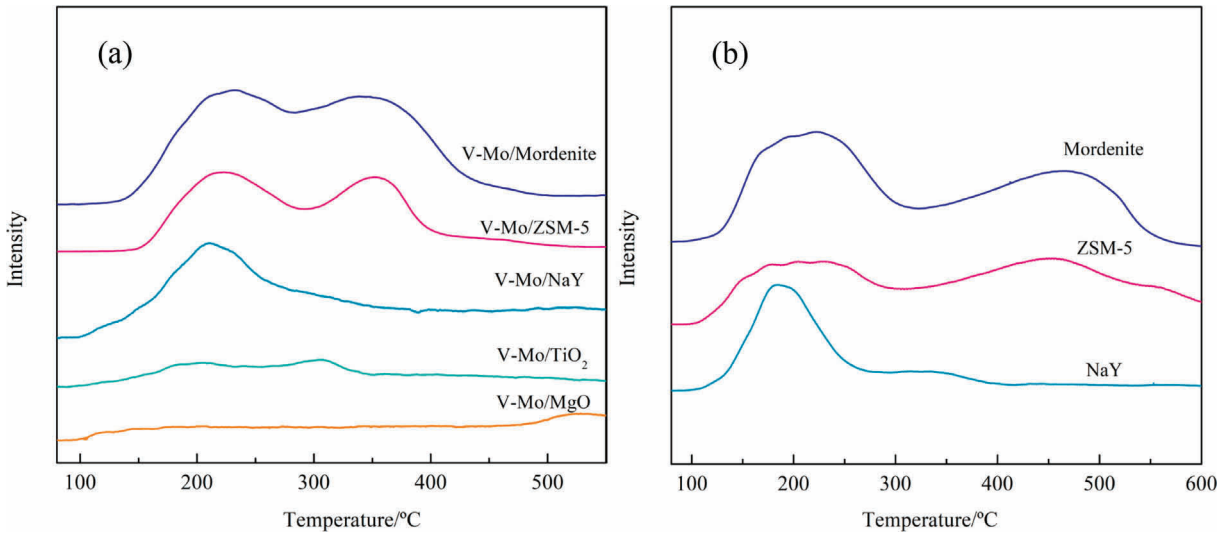

Fig. 7. NH_3-TPD spectra of (a) V-Mo catalysts with different supports and (b) various pure supports.

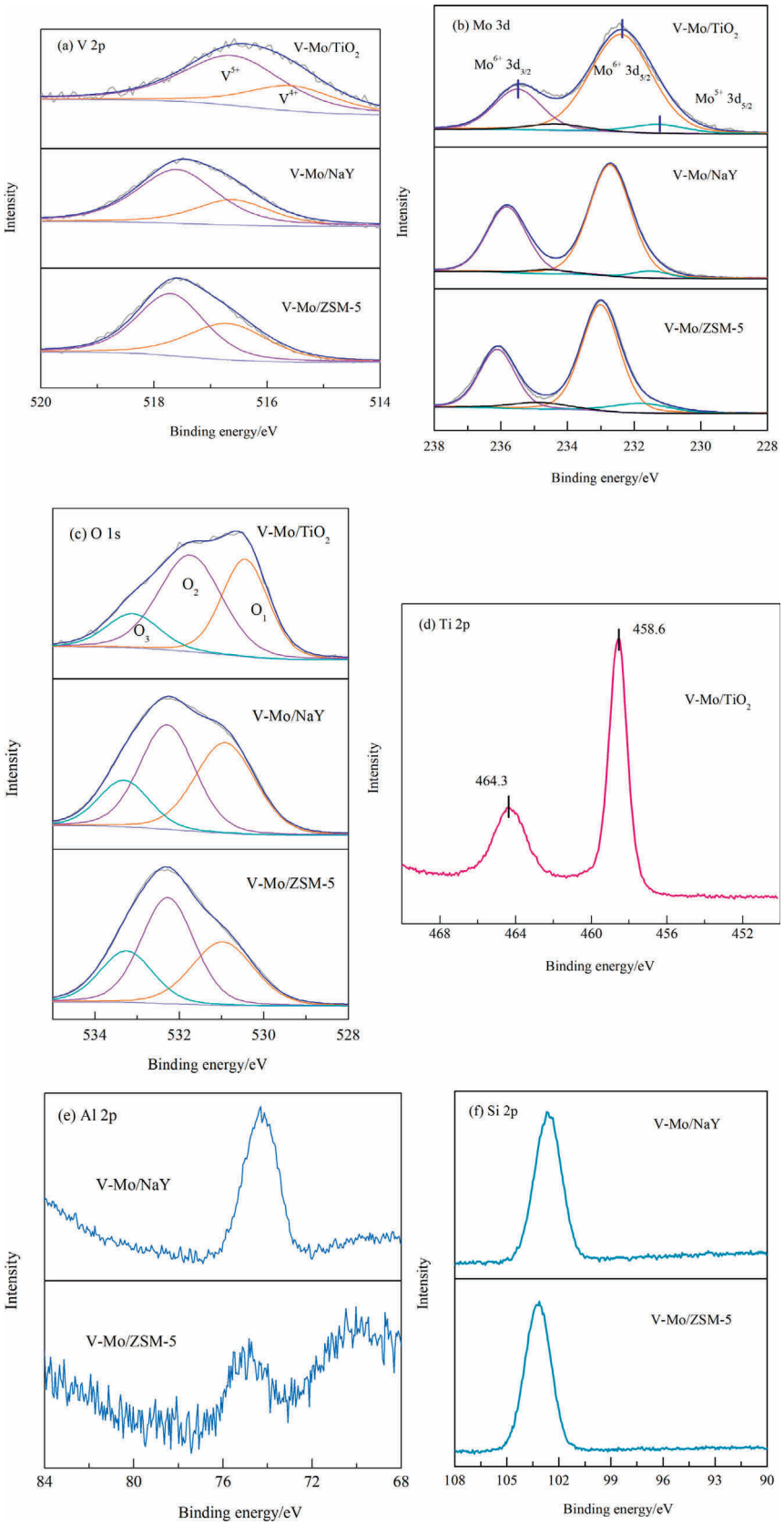

Fig. 9. XPS patterns of different catalysts: (a) V 2p; (b) Mo 3d; (c) O 1s; (d) Ti 2p; (e) Al 2p; (f) Si 2p.

MoO_x [46]. V-Mo/NaY shows higher reduction temperature by compared with V-Mo/ZSM-5 and V-Mo/TiO_2, which is related to the oxide crystal $NaVMoO_6$ on the surface of NaY [47]. For V-Mo/Mordenite, the reduction peaks near 577 and 675 °C represent the reduction of molybdena and vanadia, respectively [44]. Results show that the synergy between the two active components on

Table 2
XPS results of different components over catalysts with different supports

Catalysts	BE for V^{5+} $2p_{3/2}$/eV	V^{5+} ratio/%	BE for O_2/eV	O_2 ratio/%	BE Mo^{6+} $3d_{5/2}$/eV	Mo^{6+} ratio/%
V-Mo/TiO_2	516.6	63.8	531.8	48.8	232.4	89.9
V-Mo/NaY	517.7	69.0	532.3	41.7	232.7	94.2
V-Mo/ZSM-5	517.6	58.7	532.3	42.4	233.0	86.9

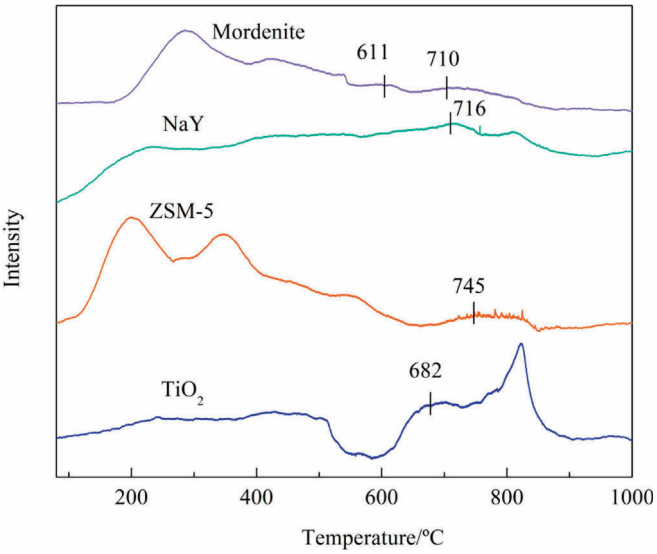

Fig. 10. O_2-TPD profiles of different VO_x-MoO_x/Support catalysts.

Mordenite is weaker, and there exists a certain amount of V_2O_5 and MoO_3 crystals on catalyst surface.

3.6. Electronic properties

The electronic structure and surface oxygen species of V-Mo/TiO_2, V-Mo/NaY and V-Mo/ZSM-5 were emphatically investigated by XPS in this section due to same Si/Al ratio in ZSM-5 and Mordenite. From Fig. 9(a), all the three catalysts contain two typical bands that represent V^{5+} and V^{4+} according to deconvolution. The significant binding energies diversities of the V^{5+} and V^{4+} indicate that the electronic environment around vanadium is different in the catalysts with different supports [48]. The $2p_{3/2}$ orbital of V^{5+} in V-Mo/TiO_2 is located at 516.6 eV, which is lower than the 517 eV in pure V_2O_5 crystal [49]. Studies have shown that when V^{5+} enters the lattice of TiO_2 to replace a Ti^{4+}, V^{5+} will attract electrons around Ti^{4+}, which will increase the outer electrons density of V^{5+} and weaken the shielding effect on inner electrons. Consequently, the $2p_{3/2}$ and $2p_{1/2}$ orbitals of V move to the low binding energy [50]. In addition, the inductive effect of V^{5+} induces the decreased electron density of Ti^{4+} and increases electron delocalization. As a result, the $2p_{3/2}$ and $2p_{1/2}$ orbitals of Ti move towards the high binding energy. Combined with the BE shifts of Ti, we can conclude some V atoms insert into the TiO_2 lattice and produce a strong interaction with supports, the electron transfer is then enhanced. However, the interaction between VO_x/MoO_x and unreducible zeolite supports is weak [51].

Table 3
Calculated Mulliken charges of O, V, Mo and Ti of V-Mo/TiO_2 (clean) and V-Mo/TiO_2 (V-Mo co-doped) by the DFT method

V-Mo/TiO_2 (clean)	Mulliken charges/e	V-Mo/TiO_2 (V-Mo co-doped)	Mulliken charges/e
1 O	−0.398	1 O	−0.426
2 O	−0.422	2 O	−0.438
3 O	−0.421	3 O	−0.436
4 O	−0.401	4 O	−0.385
5 O	−0.707	5 O	−0.711
6 O	−0.705	6 O	−0.741
1 V	1.418	1 V	1.401
2 V	1.416	2 V	1.412
1 Mo	1.912	1 Mo	1.871
2 Mo	1.908	2 Mo	1.849
1 Ti	1.672	1 Ti	1.678
2 Ti	1.657	2 Ti	1.639
3 Ti	1.659		
4 Ti	1.672	4 Ti	1.661
5 Ti	1.520	5 Ti	1.513
6 Ti	1.519	6 Ti	1.510

Fig. 9(b) shows the XPS bands for Mo 3d of different samples. Molybdenum exists in the form of Mo^{6+} and Mo^{5+}, indicating there is an electron transfer between VO_x and MoO_x: V^{4+} + Mo^{6+} ↔ V^{5+} +

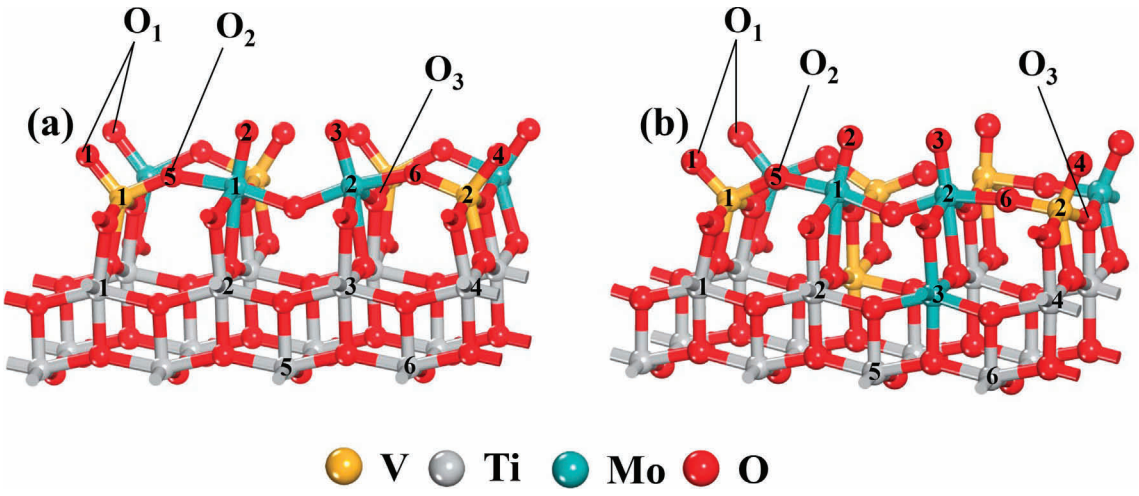

Fig. 11. Geometries of the most stable model for monolayer VO_x (50%)-MoO_x (50%) on the (0 0 1) surface of clean TiO_2 (a) and V-Mo co-doped TiO_2 (b).

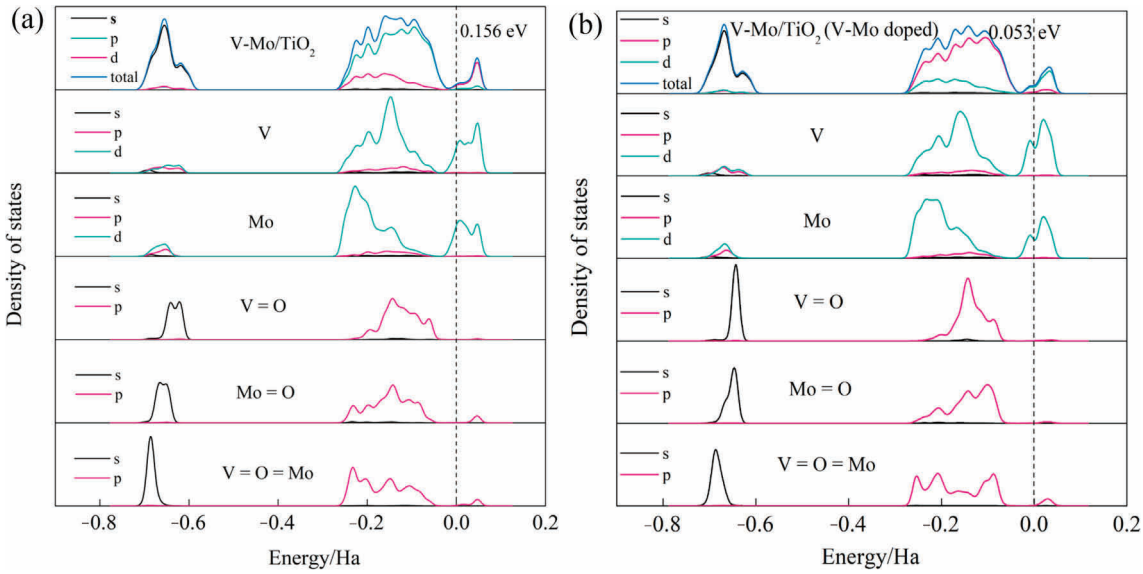

Fig. 12. PDOS of V, Mo and O of monolayer VO_x and MoO_x on (a) clean TiO_2 and (b) V-Mo co-doped TiO_2 (1 Ha = 27.212 eV).

Mo^{5+} [44,52]. Compared with pure MoO_3, the BE of Mo $3d_{5/2}$ in V-Mo/TiO_2 shifts to a lower field, which may due to the increase of outer electron density caused by Mo insertion into the adjacent V_2O_5 or TiO_2 lattice [53]. In contrast, the Mo 3d orbital of V-Mo/NaY and V-Mo/ZSM-5 show less BE offsets. From Table 2 and Fig. 9(a), (b), V-Mo/NaY has the highest content of V^{5+} and Mo^{6+} among three catalysts. And V 2p shows a larger offset than Mo 3d, suggesting that the interaction between support and VO_x is stronger. This is related to the easy formation of $AlVMoO_7$ from Al_2O_3 and V [54].

Peak fitting results and BEs of O 1s are shown in Fig. 9(c) and Table 2. Three peaks can be attributed to the lattice oxygen (O_1), oxygen vacancy (O_2) and surface-adsorbed hydroxyl (O_3), respectively [51,52,54]. V-Mo/TiO_2 contains more oxygen vacancies than V-Mo/NaY and V-Mo/ZSM-5. Vacancies can active gas oxygen after the oxygen consumption. Therefore, more reactive oxygen species means more reactive sites, and hence the catalyst shows higher activity. From Fig. 9(e), (f), 2p BE of Al and Si shifts to the higher fields, indicating that there is also an interaction between VO_x, MoO_x and zeolite supports [54].

3.7. O_2-TPD results

O_2-TPD was measured to study activity and mobility of surface oxygen. In general, for vanadia-molybdena based catalysts, oxygen desorption peaks at T < 550 °C are ascribed to the physically adsorbed oxygen and weak chemically adsorbed oxygen. Peaks at 550 °C < T < 800 °C can be attributed to chemically adsorbed oxygen on vacancies, peaks at T > 800 °C represent the lattice oxygen [55,56]. From Fig. 10, it is observed that the peak at 550 °C < T < 800 °C weakens in the order: V-Mo/TiO_2 > V-Mo/ZSM-5 > V-Mo/Mordenite ≈ V-Mo/NaY, suggesting that different supports can affect the oxygen vacancies on vanadia-molybdena based catalysts. The O_2-TPD results of oxygen adsorbed on oxygen vacancies are also consistent with the XPS results. Furthermore, V-Mo/TiO_2 shows the relative low desorption temperature than the other catalysts, indicating the higher oxygen mobility and the gas oxygen is easier to active over this catalyst [57]. According to our previous studies in organic oxidation [14], more vacancies and higher oxygen mobility stand for the fast reduction of gas oxygen and their transformation into active nucleophilic oxygen, which means the higher selectivity of target product. V-Mo/Mordenite shows two desorption peaks at around 611 and 710 °C, this may because of the weak interactions between VO_x and MoO_x, which agree with the H_2-TPR outcomes.

3.8. Theoretical calculations

From the characterization above, the advantage of TiO_2 as a support is that V and Mo can be inserted into the TiO_2 lattice to promote the catalytic performance. Therefore, to further understand the promotion effect of V-Mo co-doping in TiO_2 from the microscopic point of view, we calculated the Mulliken charges and density of states (DOS) of V-Mo/TiO_2 (clean) and V-Mo/TiO_2 (V-Mo co-doped) by the DFT method. The models of monolayer VO_x (50%) – MoO_x (50%) on the (0 0 1) surface of clean and V-Mo co-doped TiO_2 (Fig. 11) were established based on the works of Vittadini *et al.* [58]. There are three kinds of oxygens on the V-Mo/TiO_2 surface, terminal oxygen (O_1), bridging oxygen (O_2) and triply coordinated oxygen (O_3). O_3 is always inert because of their hindrances in the reaction [13,14]. Therefore, O_1 and O_2 coordinated with V and Mo are considered as the active sites.

The calculated Mulliken charges of O, V, Mo and Ti of different catalysts are shown in Table 3, and the serial number of the corresponding atom is indicated in Fig. 11. From Table 3, the Mulliken charges of V, Mo and Ti decrease after V-Mo co-doping, while the absolute value of Mulliken charges of O increase. These indicate that the electronic structures of support and active components have changed due to the electron transfer and the catalytic performance has been affected eventually. The increased absolute value of Mulliken charges of oxygen species indicates that the charge density around them increases. Generally, surface reactive oxygen species can be regarded as nucleophilic active sites in the process of methyl oxidative dehydrogenation. Therefore, oxygen species in V-Mo/TiO_2 (V-Mo co-doped) with higher electronegativity show greater catalytic activity. In addition, the activity of bridged oxygen (O_2) is higher than that of terminal oxygen (O_1).

PDOS of V, Mo and O were calculated to explore how does V and Mo insertion affect the band structure of V-Mo/TiO_2. From Fig. 12, conduction band (CB) contains unoccupied V 3d and Mo 4d orbitals, while valence band (VB) is formed from O 2p, V 3d and Mo 4d orbitals. After V-Mo co-doping in TiO_2, the band gap reduces

from 0.156 eV to 0.053 eV, which is in favor of the electron transitions and the O removal during the reaction. In addition, for V-Mo/TiO_2 (V-Mo co-doped), the V 3d and Mo 4d orbitals of CB shift to the lower energy and their states increase, suggesting the V 3d and Mo 4d unoccupied orbitals are more likely to accept electrons and the transfer of electrons from support to the active component is facilitated [59], which is in consist with the XPS results. It is possible to see that in V-Mo/TiO_2 (Mo doped) the p orbitals of O_1 (terminal oxygen) and O_2 (bridging oxygen) are at higher states in the regions closer to the Fermi level, indicating that the V and Mo insertion into TiO_2 support can improve the reactivity of surface oxygen species [59,60].

3.9. Discussion

From the characterization and catalytic testing, we can conclude that the factors that affect the catalytic effect are not unilateral. And the support not only supports the active species, but also participates in the whole catalytic process. The pore structure of catalysts shows certain effect on the reaction. More micropores in catalyst will seriously hinder the diffusion of 2-MN and 2-NA with large molecular diameter, resulting in the formation of phthalic anhydride. At the same time, the presence of microporous structure may hinder the diffusion of active cations and lead to the appearance of surface oxide crystals during the preparation of catalyst. The abundant acid sites and strong acidity on the surface of zeolite make it difficult for 2-NA to desorbed from the catalyst surface at high temperature, resulting in deep oxidation to phthalic anhydride. Poor activity of V-Mo/MgO is connected with the weak acidity and low acid concentration, indicating that the strongly basic support is not suitable for the 2-MN oxidation.

The active components-support interaction also determines the degree of VO_x and MoO_x polymerization. For TiO_2 and ZSM-5, the active components exist in the form of monolayer polymerization or a small amount of microcrystals, which results in the high 2-NA selectivity on V-Mo/TiO_2 and V-Mo/ZSM-5. However, some V_2O_5 and MoO_3 crystals exist on NaY and Mordenite surface, and lots of $NaVMoO_6$ crystals can also be detected on NaY surface due to the high Na content in NaY. Exposure of the different crystal faces of the crystal will lead to a decrease in selectivity. In addition, the acidity of crystalline oxides are stronger than that of highly dispersed ones, which will also lead to the deep oxidation of 2-NA. The interactions between supports and the active components also affect the reducibility and electron valence state of element. Weak interactions between active components and Mordenite can also lead to the independent existence of VO_x and MoO_x. Reports have shown that pure vanadia exhibits higher activity than pure molybdena and the mixed oxides. However, it is also prone to cause deep oxidation. Hence, V-Mo/Mordenite shows higher 2-MN conversion but lower 2-NA selectivity [61]. Although the active component dispersed in a monolayer on the surface of ZSM-5 provides high aldehyde selectivity, its catalytic activity is relatively weak. This is related to the lack of oxygen vacancies on its surface, the weak mobility of surface oxygen and the poor electron transport capacity within the catalyst. The different pore structures (8 MR/10 MR/12 MR) may be responsible for the different interfacial interactions of V-Mo/ZSM-5 and V-Mo/Mordenite [62]. For V-Mo/TiO_2, the insertion of V and Mo in TiO_2 lattice contributes to the higher activity of terminal and bridging oxygens.

4. Conclusions

To study how the supports affect the physicochemical properties of surface VO_x and MoO_x in the selective oxidation of 2-MN, supported vanadia-molybdena based catalysts had been prepared by using TiO_2, MgO, ZSM-5, NaY and Mordenite as supports. Results show that the factors that affect catalyst performance are manifold. The new crystalline phase $NaVMoO_6$ on NaY shows inactive performance. And the poor dispersion of VO_x and MoO_x on Mordenite due to the weak interactions leads to the low 2-NA selectivity. The stronger interactions between supports (TiO_2 and ZSM-5) and active components is in favor of the formation of monolayer VO_x and MoO_x, facilitating the production of 2-NA. In addition, V-Mo/TiO_2 shows more oxygen vacancies, higher mobility and activity of surface oxygen than the other catalysts due to the insertion of V and Mo in TiO_2 lattice, which can accelerate the activation of gas oxygen.

Data Availability

The data that has been used is confidential.

Declaration of Competing Interest

The authors declare that they have no known competing financial interests or personal relationships that could have appeared to influence the work reported in this paper.

Acknowledgements

This work was supported by Henan Province Science and Technology Research Project (232102321041).

References

[1] M. Besson, P. Gallezot, C. Pinel, Conversion of biomass into chemicals over metal catalysts, *Chem. Rev.* 114 (3) (2014) 1827–1870.
[2] H.C. Ong, W.H. Chen, A. Farooq, Y.Y. Gan, K.T. Lee, V. Ashokkumar, Catalytic thermochemical conversion of biomass for biofuel production: A comprehensive review, *Renew. Sustain. Energy Rev.* 113 (2019) 109266.
[3] D.I. Enache, J.K. Edwards, P. Landon, B. Solsona-Espriu, A.F. Carley, A.A. Herzing, M. Watanabe, C.J. Kiely, D.W. Knight, G.J. Hutchings, Solvent-free oxidation of primary alcohols to aldehydes using Au-Pd/TiO_2 catalysts, *Science* 311 (5759) (2006) 362–365.
[4] D.M. Yun, Y. Wang, J.E. Herrera, Ethanol partial oxidation over VO_x/TiO_2 catalysts: The role of titania surface oxygen on vanadia reoxidation in the mars–van Krevelen mechanism, *ACS Catal.* 8 (5) (2018) 4681–4693.
[5] J.C. Védrine, I. Fechete, Heterogeneous partial oxidation catalysis on metal oxides, *Comptes Rendus Chim.* 19 (10) (2016) 1203–1225.
[6] T. Punniyamurthy, S. Velusamy, J. Iqbal, Recent advances in transition metal catalyzed oxidation of organic substrates with molecular oxygen, *Chem. Rev.* 105 (6) (2005) 2329–2363.
[7] E. Boess, D. Sureshkumar, A. Sud, C. Wirtz, C. Farès, M. Klussmann, Mechanistic studies on a Cu-catalyzed aerobic oxidative coupling reaction with *N*-phenyl tetrahydroisoquinoline: Structure of intermediates and the role of methanol as a solvent, *J. Am. Chem. Soc.* 133 (21) (2011) 8106–8109.
[8] Z. Guo, B. Liu, Q.H. Zhang, W.P. Deng, Y. Wang, Y.H. Yang, Recent advances in heterogeneous selective oxidation catalysis for sustainable chemistry, *Chem. Soc. Rev.* 43 (10) (2014) 3480–3524.
[9] S.M. Ireland, H. Tye, M. Whittaker, Microwave-assisted multi-component synthesis of fused 3-aminoimidazoles, *Tetrahedron Lett.* 44 (23) (2003) 4369–4371.
[10] M. Bollini, J.J. Casal, A.M. Bruno, Design, synthesis, and antitumor activity of new bis-aminomethylnaphthalenes, *Bioorg. Med. Chem.* 16 (17) (2008) 8003–8010.
[11] J.W. Williams, *β*-Naphthaldehyde, *Org. Synth.* 23 (1943) 63.
[12] X.Q. Gao, F. Zhang, Y. Yu, Y.H. Dou, L. Xu, G.J. Liu, Effect of Mo loading on 2-naphthaldehyde formation from vapor phase oxidation of 2-methylnaphthalene with V_2O_5/TiO_2 catalysts, *Catal. Commun.* 122 (2019) 47–51.
[13] Y. Yu, F.F. Li, X.H. Han, S.H. Long, S.S. Shi, L. Xu, G.J. Liu, High-performance metal oxide-modified V/TiO_2 catalysts for selective oxidation of 2-methylnaphthalene to 2-naphthaldehyde: An experimental and theoretical study, *Ind. Eng. Chem. Res.* 60 (8) (2021) 3435–3451.
[14] L.D. Ellis, J. Ballesteros-Soberanas, D.K. Schwartz, J.W. Medlin, Effects of metal oxide surface doping with phosphonic acid monolayers on alcohol dehydration activity and selectivity, *Appl. Catal. A* 571 (2019) 102–106.
[15] X.J. Wang, X. Zhang, P. Li, K.I. Otake, Y.X. Cui, J.F. Lyu, M.D. Krzyaniak, Y.Y. Zhang, Z.Y. Li, J. Liu, C.T. Buru, T. Islamoglu, M.R. Wasielewski, Z. Li, O.K. Farha, Vanadium catalyst on isostructural transition metal, lanthanide, and actinide based metal-organic frameworks for alcohol oxidation, *J. Am. Chem. Soc.* 141 (20) (2019) 8306–8314.

[16] Y. Ganjkhanlou, T.V.W. Janssens, P.N.R. Vennestrøm, L. Mino, M.C. Paganini, M. Signorile, S. Bordiga, G. Berlier, Location and activity of VO_x species on TiO_2 particles for NH_3-SCR catalysis, *Appl. Catal. B* 278 (2020) 119337.
[17] J.F. Pang, M. Yin, P.F. Wu, X.Q. Li, H.Y. Li, M.Y. Zheng, T. Zhang, Advances in catalytic dehydrogenation of ethanol to acetaldehyde, *Green Chem.* 23 (20) (2021) 7902–7916.
[18] V.V. Kaichev, Y.A. Chesalov, A.A. Saraev, A.Y. Klyushin, A. Knop-Gericke, T.V. Andrushkevich, V.I. Bukhtiyarov, Redox mechanism for selective oxidation of ethanol over monolayer V_2O_5/TiO_2 catalysts, *J. Catal.* 338 (2016) 82–93.
[19] L. Artiglia, S. Agnoli, G. Granozzi, Vanadium oxide nanostructures on another oxide: The viewpoint from model catalysts studies, *Coord. Chem. Rev.* 301–302 (2015) 106–122.
[20] W.C. Vining, J. Strunk, A.T. Bell, Investigation of the structure and activity of $VO_x/ZrO_2/SiO_2$ catalysts for methanol oxidation to formaldehyde, *J. Catal.* 281 (2) (2011) 222–230.
[21] T.V. Andrushkevich, V.V. Kaichev, Y.A. Chesalov, A.A. Saraev, V.I. Buktiyarov, Selective oxidation of ethanol over vanadia-based catalysts: The influence of support material and reaction mechanism, *Catal. Today* 279 (2017) 95–106.
[22] I.E. Wachs, Catalysis science of supported vanadium oxide catalysts, *Dalton Trans* 42 (2013) 11762–11769.
[23] B. Beck, M. Harth, N.G. Hamilton, C. Carrero, J.J. Uhlrich, A. Trunschke, S. Shaikhutdinov, H. Schubert, H.J. Freund, R. Schlögl, J. Sauer, R. Schomäcker, Partial oxidation of ethanol on vanadia catalysts on supporting oxides with different redox properties compared to propane, *J. Catal.* 296 (2) (2012) 120–131.
[24] V.V. Kaichev, G.Y. Popova, Y.A. Chesalov, A.A. Saraev, D.Y. Zemlyanov, S.A. Beloshapkin, A. Knop-Gericke, R. Schlögl, T.V. Andrushkevich, V.I. Bukhtiyarov, Selective oxidation of methanol to form dimethoxymethane and methyl formate over a monolayer V_2O_5/TiO_2 catalyst, *J. Catal.* 311 (2014) 59–70.
[25] F. Chandoul, A. Boukhachem, F. Hosni, H. Moussa, M.S. Fayache, M. Amlouk, R. Schneider, Change of the properties of nanostructured MoO_3 thin films using gamma-ray irradiation, *Ceram. Int.* 44 (11) (2018) 12483–12490.
[26] R. Zhu, A. Chatzidimitriou, J.Q. Bond, Influence of vanadate structure and support identity on catalytic activity in the oxidative cleavage of methyl ketones, *J. Catal.* 359 (2018) 171–183.
[27] G.C. Bond, S.F. Tahir, ChemInform abstract: Vanadium oxide monolayer catalysts. preparation, characterization, and catalytic activity, *ChemInform* 22 (43) (1991) 1–31.
[28] C.A. Carrero, R. Schloegl, I.E. Wachs, R. Schomaecker, Critical literature review of the kinetics for the oxidative dehydrogenation of propane over well-defined supported vanadium oxide catalysts, *ACS Catal.* 4 (10) (2014) 3357–3380.
[29] K. Shimura, T. Fujitani, Effects of promoters on the performance of a VO_x/SiO_2 catalyst for the oxidation of methane to formaldehyde, *Appl. Catal. A* 577 (2019) 44–51.
[30] E.V. Kondratenko, T. Peppel, D. Seeburg, V.A. Kondratenko, N. Kalevaru, A. Martin, S. Wohlrab, Methane conversion into different hydrocarbons or oxygenates: Current status and future perspectives in catalyst development and reactor operation, *Catal. Sci. Technol.* 7 (2) (2017) 366–381.
[31] P. Eversfield, T. Lange, M. Hunger, E. Klemm, Selective oxidation of *o*-xylene to phthalic anhydride on tungsten, tin, and potassium promoted VO_x on TiO_2 monolayer catalysts, *Catal. Today* 333 (2019) 120–126.
[32] I.E. Wachs, S.S. Chan, C.C. Chersich, R.Y. Saleh, The interaction of V_2O_5 with TiO_2(anatase): the active site for the oxidation of *O*-xylene to phthalic anhydride, Elsevier, Amsterdam, 1984, pp. 275–282.
[33] H.Y. Zhao, S. Bennici, J.Y. Shen, A. Auroux, Nature of surface sites of V_2O_5–TiO_2/SO_4^{2-} catalysts and reactivity in selective oxidation of methanol to dimethoxymethane, *J. Catal.* 272 (1) (2010) 176–189.
[34] M. Gómez-Cazalilla, J.M. Mérida-Robles, A. Gurbani, E. Rodríguez-Castellón, A. Jiménez-López, Characterization and acidic properties of Al-SBA-15 materials prepared by post-synthesis alumination of a low-cost ordered mesoporous silica, *J. Solid State Chem.* 180 (3) (2007) 1130–1140.
[35] B.M. Reddy, I. Ganesh, B. Chowdhury, Design of stable and reactive vanadium oxide catalysts supported on binary oxides, *Catal. Today* 49 (1–3) (1999) 115–121.
[36] M.O. Guerrero-Pérez, M.C. Herrera, I. Malpartida, M.A. Larrubia, L.J. Alemany, Characterization and FT-IR study of nanostructured alumina-supported V-Mo-W-O catalysts, *Catal. Today* 118 (3–4) (2006) 360–365.
[37] Y. Liu, X.B. Ma, S.P. Wang, J.L. Gong, The nature of surface acidity and reactivity of MoO_3/SiO_2 and MoO_3/TiO_2-SiO_2 for transesterification of dimethyl oxalate with phenol: A comparative investigation, *Appl. Catal. B* 77 (1–2) (2007) 125–134.
[38] H.L. Koh, H.K. Park, Characterization of MoO_3-V_2O_5/Al_2O_3 catalysts for selective catalytic reduction of NO by NH_3, *J. Ind. Eng. Chem.* 19 (1) (2013) 73–79.
[39] S.W. Yang, E. Iglesia, A.T. Bell, Oxidative dehydrogenation of propane over $V_2O_5/MoO_3/Al_2O_3$ and $V_2O_5/Cr_2O_3/Al_2O_3$: Structural characterization and catalytic function, *J. Phys. Chem. B* 109 (18) (2005) 8987–9000.
[40] M.A. Bañares, S.J. Khatib, Structure-activity relationships in alumina-supported molybdena-vanadia catalysts for propane oxidative dehydrogenation, *Catal. Today* 96 (4) (2004) 251–257.
[41] X.A. Li, J.H. Li, Y.E. Peng, X.S. Li, K.Z. Li, J.M. Hao, Comparison of the structures and mechanism of arsenic deactivation of CeO_2–MoO_3 and CeO_2–WO_3 SCR catalysts, *J. Phys. Chem. C* 120 (32) (2016) 18005–18014.
[42] X.M. Huang, Y.G. Li, Y.D. Xu, W.J. Shen, Kinetics of selective oxidation of dimethyl ether to formaldehyde over Al_2O_3-supported VO_x and MoO_x catalysts, *Catal. Lett.* 97 (3–4) (2004) 185–190.
[43] W. Luo, J. Rong, W.X. Zhao, K.K. Kang, L.L. Long, X.J. Yao, Morphology and crystal-plane dependence of CeO_2-TiO_2 catalysts: Activity and mechanism for the selective catalytic reduction of NO_x with NH_3, *Chem. Eng. J.* 444 (2022) 136488.
[44] J. Kim, E.E. Kwon, J.E. Lee, S.H. Jang, J.K. Jeon, J. Song, Y.K. Park, Effect of zeolite acidity and structure on ozone oxidation of toluene using Ru-Mn loaded zeolites at ambient temperature, *J. Hazard. Mater.* 403 (2021) 123934.
[45] J. Arfaoui, A. Ghorbel, C. Petitto, G. Delahay, Novel V_2O_5-CeO_2-TiO_2-SO_4^{2-} nanostructured aerogel catalyst for the low temperature selective catalytic reduction of NO by NH_3 in excess O_2, *Appl. Catal. B* 224 (2018) 264–275.
[46] R. Kuma, T. Kitano, T. Tsujiguchi, T. Tanaka, Effect of molybdenum on the structure and performance of V_2O_5/TiO_2-SiO_2-MoO_3 catalysts for the oxidative degradation of *o*-chlorotoluene, *Appl. Catal. A* 595 (2020) 117496.
[47] M.A. Bañares, N.D. Spencer, M.D. Jones, I.E. Wachs, Effect of alkali metal cations on the structure of catalysts and its relevance to the selective oxidation of methane and methanol, *J. Catal.* 146 (1) (1994) 204–210.
[48] Z.M. Liu, S.X. Zhang, J.H. Li, J.Z. Zhu, L.L. Ma, Novel V_2O_5-CeO_2/TiO_2 catalyst with low vanadium loading for the selective catalytic reduction of NO_x by NH_3, *Appl. Catal. B* 158–159 (2014) 11–19.
[49] J. Mendialdua, R. Casanova, Y. Barbaux, XPS studies of V_2O_5, V_6O_{13}, VO_2 and V_2O_3, *J. Electron Spectrosc. Relat. Phenom.* 71 (3) (1995) 249–261.
[50] Y. Qiu, B. Liu, J. Du, Q. Tang, Z.H. Liu, R.L. Liu, C.Y. Tao, The monolithic cordierite supported V_2O_5-MoO_3/TiO_2 catalyst for NH_3-SCR, *Chem. Eng. J.* 294 (2016) 264–272.
[51] M.V. Ganduglia-Pirovano, C. Popa, J. Sauer, H. Abbott, A. Uhl, M. Baron, D. Stacchiola, O. Bondarchuk, S. Shaikhutdinov, H.J. Freund, Role of ceria in oxidative dehydrogenation on supported vanadia catalysts, *J. Am. Chem. Soc.* 132 (7) (2010) 2345–2349.
[52] S.J. Khatib, R. Guil-López, M.A. Peña, J.L.G. Fierro, M.A. Bañares, Alumina-supported V-Mo-O mixed oxide catalysts, the formation of phases involving aluminum: $AlVMoO_7$, *Catal. Today* 118 (3–4) (2006) 353–359.
[53] X.W. Lou, H.C. Zeng, Complex alpha-$MoO_{(3)}$ nanostructures with external bonding capacity for self-assembly, *J. Am. Chem. Soc.* 125 (9) (2003) 2697–2704.
[54] Y.L. Meng, T. Wang, S. Chen, Y.J. Zhao, X.B. Ma, J.L. Gong, Selective oxidation of methanol to dimethoxymethane on V_2O_5-MoO_3/γ-Al_2O_3 catalysts, *Appl. Catal. B* 160–161 (2014) 161–172.
[55] C. Li, K. Domen, K.I. Maruya, T. Onishi, IR spectra of dioxygen species formed on CeO_2 at room temperature, *J. Chem. Soc., Chem. Commun.* 23 (1988) 1541.
[56] B. Pongthawornsakun, S. Phatyenchuen, J. Panpranot, P. Praserthdam, The low temperature selective oxidation of H_2S to elemental sulfur on TiO_2 supported V_2O_5 catalysts, *J. Environ. Chem. Eng.* 6 (1) (2018) 1414–1423.
[57] V.D. Sokolovskii, Principles of oxidative catalysis on solid oxides, *Catal. Rev.* 32 (1–2) (1990) 1–49.
[58] A. Vittadini, M. Casarin, M. Sambi, A. Selloni, First-principles studies of vanadia-titania catalysts: Beyond the monolayer, *J. Phys. Chem. B* 109 (46) (2005) 21766–21771.
[59] A. Suarez Negreira, J. Wilcox, Role of WO_3 in the Hg oxidation across the V_2O_5–WO_3–TiO_2 SCR catalyst: A DFT study, *J. Phys. Chem. C* 117 (46) (2013) 24397–24406.
[60] Y. Zhang, H.R. Guo, J.K. Ren, X.P. Li, W.L. Ren, R. Song, MoO_3 crystal facets modulation by doping heteroatom Fe from polyoxometalate for quasi-industrial oxygen evolution reaction, *Appl. Catal. B* 298 (2021) 120582.
[61] M. Faraldos, M.A. Bañares, J.A. Anderson, H.C. Hu, I.E. Wachs, J.L.G. Fierro, Comparison of silica-supported MoO_3 and V_2O_5 Catalysts in the selective partial oxidation of methane, *J. Catal.* 160 (2) (1996) 214–221.
[62] G. Brezicki, J. Zheng, C. Paolucci, R. Schlögl, R.J. Davis, Effect of the co-cation on Cu speciation in Cu-exchanged mordenite and ZSM-5 catalysts for the oxidation of methane to methanol, *ACS Catal.* 11 (9) (2021) 4973–4987.